

Cross Kerr Effect Induced by Coupled Josephson Qubits in Circuit Quantum Electrodynamics

Yong Hu* and Guo-Qin Ge†

*School of Physics, Huazhong University of Science
and Technology, Wuhan, Hubei 430074, China*

Shi Chen and Xiao-Fei Yang

*Department of Electronic Science and Technology,
Huazhong University of Science and Technology, Wuhan, Hubei 430074, China*

You-Ling Chen

Department of Physics, Peking University, Beijing 100871, China

Abstract

We propose a scheme for implementing cross Kerr nonlinearity between two superconducting transmission line resonators (TLR) via their interaction with a coupler which is constructed by two superconducting charge qubits connected to each other via a superconducting quantum interference device. When suitably driven, the coupler can induce very strong cross phase modulation (XPM) between the two TLRs due to its N-type level structure and the consequent electromagnetically induced transparency in its lowest states. The flexibility of our design can lead to various inter-TLR coupling configurations. The obtained cross Kerr coefficient is large enough to allow many important quantum operations in which only few photons are involved. We further show that this scheme is very robust against the fluctuations in solid state circuits. Our numerical calculations imply that the absorption and dispersion resulted from the decoherence of the coupler are very small compared with the strength of the proposed XPM.

PACS numbers: 03.67.Lx, 03.67.Bg, 42.50.Pq

*Electronic address: yhu3@ustc.edu.cn

†Electronic address: gqge@mail.hust.edu.cn

I. INTRODUCTION

The circuit quantum electrodynamics (QED) [1, 2] which employs the superconducting coplanar transmission line resonator (TLR) to substitute the standing-wave optical cavity and superconducting qubits [3–5] to replace the atoms is an on-chip realization of cavity QED [6]. Compared with conventional optical implementations, this solid-state architecture offers unprecedented tunability and scalability which are leading to flexible quantum optics in electronic circuits. Since the strong coupling between the TLRs and the superconducting qubits with vacuum Rabi frequency up to three orders larger than the qubit decoherence and cavity decay has already been achieved [7, 8], many important quantum information processes (QIP), including coupling qubits using the TLR as a data bus [10, 11] and preparing the TLR Fock states [9, 12, 13] have been demonstrated.

Stimulated by the advances on the single TLR level, recently the ideas of photon manipulations between TLRs have been developed [15–17]. The motivation is to facilitate the future realization of scalable quantum computation. These schemes mainly consider a model of two TLRs coupled to an assistant tunable coupler. One can tune on and off the individual energy transfer between the TLRs and the coupler through frequency selection and thus manipulate the two mode photon states. A very latest experiment have realized the NOON state preparation in two TLRs connected to an entanglement generator [18].

In optical systems, besides the linear tight-binding photon transfer, the nonlinear Kerr interaction between cavity modes has also been studied extensively. The cross Kerr nonlinearity, or the so-called cross phase modulation (XPM), has found wide application in QIPs including the construction of nontrivial quantum gates [21–23], the preparation of entangled photon states [24, 34], and quantum non-demolition measurement [25]. Enhancement of dissipation-free photon-photon interactions at the few-photon level is a fundamental challenge in quantum optics. Since photons can hardly interact with each other, the XPM is often obtained by coupling two photon modes to an atomic nonlinear media. To minimize the dispersion and absorption, schemes of exploiting destructive quantum coherence in N type atoms have been proposed [26] and realized [27–29]. The reported experiments are performed in the semiclassical region due to the very small interaction strength between the laser fields and ^{87}Rb atoms, which is often on the same level of the atomic decoherence rates. In order to obtain significant phase shift, the probe and control pulses contain large numbers

of photons. The weak coupling places a major hindrance to the further application of the Kerr effect on the single photon level.

In this paper, we aim at the realization of strong cross Kerr coupling between two TLR modes. This work is inspired by the recent self phase modulation scheme in circuit QED system [41]. We design a superconducting circuit which exhibits complete analogy to the N level XPM schemes in atomic systems. The proposed four level artificial molecule is constructed by two Josephson charge qubits coupled by a superconducting quantum interference device (SQUID). When capacitively coupled to the two TLRs, the molecule induces cross Kerr interaction between microwave photons in the two TLRs. The strong TLR-molecule coupling can boost the XPM strength up to several MHz. Moreover, the dispersion and absorption resulted from the decoherence of the coupler are estimated to be negligible compared with the obtained XPM strength. Our system is flexible enough to allow various inter-TLR coupling configurations. Since long lifetimes for both the TLRs and the molecule have already been achieved, many QIPs between the TLRs in which there are only few photons involved can be performed with very high fidelities.

The paper is organized in the following manner. We first briefly describe the general N-type scheme of XPM in Sec. II and then study its realization in circuit QED system in Sec. III. In Sec. IV, the influence of the decoherence on the XPM scheme is investigated in detail. The application of our XPM scheme and the related discussion are presented in Sec. V, while the conclusion is given in Sec. VI

II. XPM INDUCED BY THE N TYPE ATOM

We start from the theoretical model of two cavity modes, labeled by their annihilation operators a_1 and a_2 , coupled to an atom with N type level structure, as shown in Fig. 1. The first mode couples the $|1\rangle \leftrightarrow |3\rangle$ transition with strength g_1 and detuning δ , while the second mode couples the $|2\rangle \leftrightarrow |4\rangle$ with strength g_2 and detuning Δ . In addition, a classical laser field is applied to drive the $|2\rangle \leftrightarrow |3\rangle$ transition with strength Ω_c . The frequency of the classical field is set to be in Raman resonance with the first mode. In the interaction picture, the Hamiltonian of the system can be written as

$$H_{sys} = H_{atom} + H_{int}, \quad (1)$$

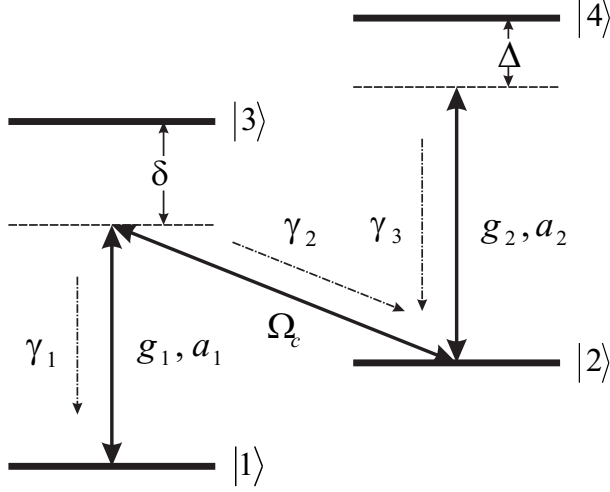


FIG. 1: (Color online). The N scheme for cross Kerr interaction. Two cavity modes a_1 and a_2 induce the transitions $|1\rangle \rightarrow |3\rangle$ and $|2\rangle \rightarrow |4\rangle$ of the N type atom with coupling strength g_1 and g_2 respectively. The δ and Δ are the corresponding detunings, while the factors γ_1 , γ_2 , and γ_3 label the decay rates from the upper levels to the lower levels. In addition, an external pumping pulse couples $|2\rangle$ and $|3\rangle$ with Rabi frequency Ω_c . The classical pumping is set to be in dark resonance with the first cavity mode so that the states $|1\rangle$, $|2\rangle$ and $|3\rangle$ exhibit electromagnetically induced transparency.

with

$$H_{atom} = \delta\sigma_{33} + \Delta\sigma_{44}, \quad (2)$$

$$H_{int} = i[g_1(a_1^\dagger\sigma_{13} - \sigma_{31}a_1) + g_2(a_2^\dagger\sigma_{24} - \sigma_{42}a_2) + \Omega_c(\sigma_{23} - \sigma_{32})], \quad (3)$$

where $\sigma_{jk} = |j\rangle\langle k|$ are the atomic raising and lowering operators for $j \neq k$ and population operators for $j = k$. In the limit [30–32]

$$\left|\frac{g_1}{\Omega_c}\right|^2 \ll 1, |g_2| \ll |\Delta|, \quad (4)$$

the atom evolves rapidly on the time scales relevant for the cavities. After the adiabatical elimination of the atomic degrees of freedom, an effective Kerr photon-photon interaction

$$H_{sys} \cong H_{eff} = -\frac{g_2^2 g_1^2}{\Delta \Omega_c^2} a_1^\dagger a_1 a_2^\dagger a_2, \quad (5)$$

can be obtained [26].

The Kerr effect induced by the N type atoms has been investigated in the past few years [19, 22, 26–29]. The physics of H_{eff} can be interpreted in an intuitive way: Suppose initially the atom is in its ground state $|1\rangle$. In the first step we set $g_2 = 0$ so that $|1\rangle$, $|2\rangle$ and $|3\rangle$ decouple from $|4\rangle$. When the classical pumping is added, the states $|1\rangle$ and $|2\rangle$ form a dark state, in which the destructive quantum interference between the $|1\rangle \leftrightarrow |3\rangle$ and $|2\rangle \leftrightarrow |3\rangle$ transition branches cancels the dispersion and absorption [35] of the a_1 mode. The stationary population on the level $|2\rangle$ is thus determined by the photon number $a_1^\dagger a_1$ as

$$\langle \sigma_{22} \rangle \cong g_1^2 a_1^\dagger a_1 / \Omega_c^2. \quad (6)$$

When the second mode is added back to couple the $|3\rangle \leftrightarrow |4\rangle$ transition dispersively, the resulting AC Stark shift has the form $-g_2^2 a_2^\dagger a_2 \sigma_{22} / \Delta = -g_1^2 g_2^2 a_1^\dagger a_1 a_2^\dagger a_2 / (\Delta \Omega_c^2)$.

Mathematically, to derive H_{eff} , we first write the evolution equations of the operators a_1 and a_2 as

$$\frac{da_1}{dt} = g_1 \sigma_{13} - \kappa_1 a_1 - \sqrt{2\kappa_1} a_{1in}(t), \quad (7)$$

$$\frac{da_2}{dt} = g_2 \sigma_{24} - \kappa_2 a_2 - \sqrt{2\kappa_2} a_{2in}(t), \quad (8)$$

where $\kappa_{1,2}$ are the decay rates of the cavities, and $a_{1,2in}(t)$ are the input noise operators [20, 33]. Adiabatic elimination of the atom allows us to express the atomic operators in terms of the mode operators. Formally this is accomplished by setting the time derivatives of all the σ_{jk} to be zero. The stationary values $\langle \sigma_{jk} \rangle_S$ of the atomic operators σ_{jk} can be expanded as

$$\langle \sigma_{jk} \rangle_S \cong \sum_{n=0}^{\infty} \sigma_{jk}^n \quad (9)$$

where σ_{jk}^n contains the multiplication of n creation or annihilation operators of the cavities. We further use $\sigma_{11} = 1$ as the starting value and iteratively determine the remaining coefficients of the expansion. We thus get

$$\langle \sigma_{13} \rangle_S = -\frac{g_1 g_2^2}{i \Delta \Omega_c^2} a_2^\dagger a_1 a_2, \quad (10)$$

$$\langle \sigma_{24} \rangle_S = -\frac{g_1^2 g_2}{i \Delta \Omega_c^2} a_1^\dagger a_1 a_2. \quad (11)$$

Replacing σ_{13} and σ_{24} in Eqs. (7) and (8) by their stationary values in Eqs. (10) and (11) we obtain

$$\frac{da_1}{dt} = -\frac{g_1^2 g_2^2}{i \Delta \Omega_c^2} a_2^\dagger a_1 a_2 - \kappa_1 a_1 - \sqrt{2\kappa_1} a_{1in}(t), \quad (12)$$

$$\frac{da_2}{dt} = -\frac{g_1^2 g_2^2}{i\Delta\Omega_c^2} a_1^\dagger a_1 a_2 - \kappa_2 a_2 - \sqrt{2\kappa_2} a_{2in}(t). \quad (13)$$

The first terms in Eq. (12) and (13) yield an effective Kerr interaction

$$H_{eff} = -\eta a_2^\dagger a_1^\dagger a_1 a_2, \quad (14)$$

where $\eta = g_1^2 g_2^2 / (\Delta\Omega_c^2)$ is the Kerr coefficient.

The first order terms in the expansion of $\langle\sigma_{13}\rangle_S$ and $\langle\sigma_{24}\rangle_S$ which represent the linear dispersion and absorption of the two cavities, are vanishing. The suppression of linear susceptibilities is a result of the quantum phase coherence in the atom [35]. When the decoherence of the atom is taken into account, the phase coherence is broken and the linear susceptibilities become nonzero. Also, the third order susceptibility η is modified from real to complex. The derivation of Eqs. (10) and (11) and the discussions about the influence of the atomic decoherence are provided in the forthcoming sections and the Appendix.

III. THE N SCHEME IN CIRCUIT QED

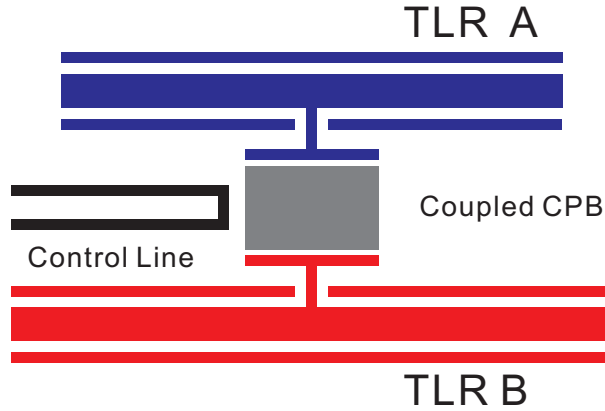


FIG. 2: (Color online). Schematic circuit for XPM between two TLRs. The TLR A (blue) and the TLR B (red) are capacitively connected to a superconducting molecule (gray) controlled by an external circuit (black).

The N scheme described in Sec. II can be realized in superconducting quantum circuits. We consider a system of two TLRs capacitively coupled to an artificial superconducting molecule, as shown in Fig. 2. In the following subsections we explicitly show that all the required ingredients of the N level XPM proposal can be established in the circuit QED system.

A. The superconducting molecule: an artificial N type system

The artificial molecule in Fig. 2 is constructed by two superconducting Cooper pair boxes (CPB) [36, 42] coupled by a SQUID [37], as sketched in Fig. 3. Each CPB consists of a small superconducting island connected to the ground electrode by a symmetric SQUID with capacitance C_{J_i} and tunable Josephson coupling energy E_{J_i} for $i = 1, 2$. The gate voltages V_{g_i} bias the corresponding qubits via the gate capacitors C_{g_i} . Finally, the CPBs are connected to each other by a coupling SQUID with capacitance C_m and Josephson energy E_{J_m} . The Hamiltonian of the molecule reads

$$H_0 = 4E_m(n_1 - n_{g1})(n_2 - n_{g2}) - E_{J_m} \cos(\Phi_1 - \Phi_2) + \sum_{i=1,2} [E_{c_i}(n_i - n_{g_i})^2 - E_{J_i} \cos \Phi_i], \quad (15)$$

where $n_{g_{1,2}} = C_{g_{1,2}}V_{g_{1,2}}/2e$ denote the gate-induced charge numbers on the CPBs, $\Phi_{1,2}$ are the canonical conjugate variables to $n_{1,2}$, $E_{c_{1,2}} = 2e^2C_{\Sigma 2,1}/(C_{\Sigma 1}C_{\Sigma 2} - C_m^2)$ are the effective Cooper-pair charging energies ($C_{\Sigma i} = C_{g_i} + C_{J_i} + C_m$ is the sum of all capacitances around the i th qubit), and $E_m = e^2C_m/(C_{\Sigma 1}C_{\Sigma 2} - C_m^2)$ is the capacitive coupling strength between the CPBs. Near the co-degeneracy point $n_{g1} = n_{g2} = 1/2$, we can use the two-level language

$$n_i = (1 + \sigma_{xi})/2, \cos \Phi_i = -\sigma_{zi}/2, \quad (16)$$

for $i = 1, 2$, to describe the molecule as

$$H_0 = E_m[\sigma_{x1}\sigma_{x2} - b_0(\sigma_{z1}\sigma_{z2} + \sigma_{y1}\sigma_{y2})] + \frac{1}{2} \sum_{i=1,2} [E_{b_i}\sigma_{xi} + E_{J_i}\sigma_{zi}], \quad (17)$$

where $E_{b_{1,2}} = 2[E_{c_{1,2}}(1 - 2n_{g_{1,2}}) + E_m(1 - 2n_{g_{2,1}})]$ are the effective charge biases, and $b_0 = E_{J_m}/4E_m$.

Being a Coulomb blockade device, the coupled-CPBs is very sensitive to noise from charge degrees of freedom [43, 52]. By operating the molecule at its optimal point, chosen such that the linear longitudinal qubits-noise coupling vanishes, we can prolong its dephasing times by several orders [42]. For this reason, here we concentrate on the behavior of the coupled CPBs at the co-degeneracy point $n_{g1} = n_{g2} = 1/2$, which can be verified as the optimal point later. Without loss of generality, we further assume that the two CPBs are identical,

i. e. $E_{J1} = E_{J2} = E_J$, $C_{J1} = C_{J2} = C_J$, and $C_{\Sigma1} = C_{\Sigma2} = C_{\Sigma}$. In this situation, the eigenstates and eigenvalues of H_0 can be written as

$$\begin{aligned}
|1\rangle &= -\sin\theta|00\rangle + \cos\theta|11\rangle, \\
|2\rangle &= (-|01\rangle + |10\rangle)/\sqrt{2}, \\
|3\rangle &= (|01\rangle + |10\rangle)/\sqrt{2}, \\
|4\rangle &= \cos\theta|00\rangle + \sin\theta|11\rangle,
\end{aligned}
\tag{18}$$

$$\begin{aligned}
E_1 &= -E_{mN} - E_m b_0, \\
E_2 &= -E_m(1 - 2b_0), \\
E_3 &= E_m, \\
E_4 &= E_{mN} - E_m b_0.
\end{aligned}
\tag{19}$$

where $E_{mN} = \sqrt{E_J^2 + E_m^2(1 - b_0)^2}$, $E = \sqrt{E_J^2 + E_m^2}$, and $\theta = [\arcsin(E_m/E) + \arcsin(E_J b_0/2E_{mN})]/2$.

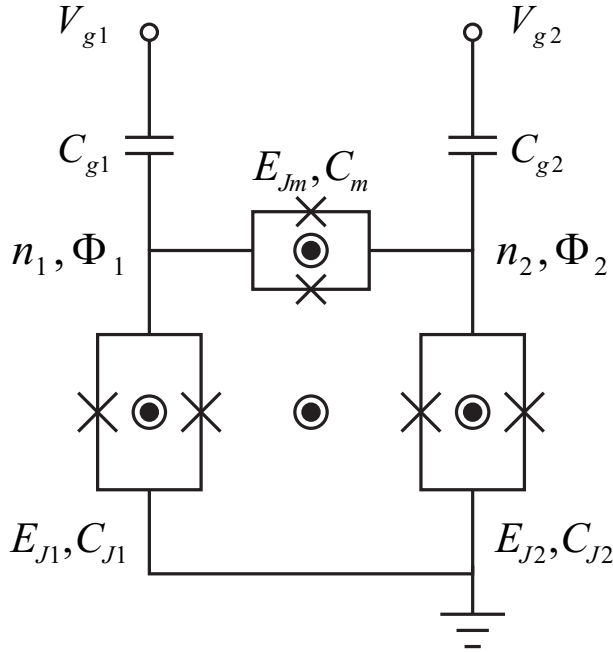


FIG. 3: (Color online). Schematic plot of the coupled CPBs. The crosses label the Josephson junctions, while the round circle in the SQUID loops represent the penetrating flux.

The levels $\{|1\rangle, |2\rangle, |3\rangle, |4\rangle\}$ in Eq. (18) have the required N configuration in Sec. II and can be mapped to the four states in Fig. 1 one by one. In experiments, E_J is often larger than E_m , while the maximum of b_0 is usually on the order of unity. We thus can

modify the rough energy scale of the molecule by tuning E_J . Moreover, b_0 can be used to control the details of the energy structure. When $b_0 = 0$, the N level is symmetric, i. e. $E_4 - E_2 = E_3 - E_1$. Tuning b_0 to non-zero value can break the symmetry. The influences of b_0 on the level spacings $E_{42} = E_4 - E_2$, $E_{31} = E_3 - E_1$, and $E_{32} = E_3 - E_2$ are shown in Fig. 4. In this calculation, we set the parameters of the coupled CPBs as $E_J/2\pi = 20$ GHz and $E_m/2\pi = 5$ GHz [39, 40]. As plotted in Fig. 4, the level spacings go through very large range when b_0 varies in the region $b_0 \in [0, 0.8]$. Therefore, with the tunability of b_0 and E_J , the level splits of the molecule can be modulated at will. We further notice that the co-degeneracy bias point $n_{g1} = n_{g2} = 1/2$ remains to be the optimal point for the molecule during the tuning of b_0 . The operators σ_{x1} and σ_{x2} , through which the system couples to the charge noise, have the form

$$\sigma_{x1} = \begin{bmatrix} 0 & -\sin\phi & \cos\phi & 0 \\ -\sin\phi & 0 & 0 & \cos\phi \\ \cos\phi & 0 & 0 & \sin\phi \\ 0 & \cos\phi & \sin\phi & 0 \end{bmatrix}, \quad (20)$$

$$\sigma_{x2} = \begin{bmatrix} 0 & \sin\phi & \cos\phi & 0 \\ \sin\phi & 0 & 0 & -\cos\phi \\ \cos\phi & 0 & 0 & \sin\phi \\ 0 & -\cos\phi & \sin\phi & 0 \end{bmatrix}, \quad (21)$$

where $\phi = \theta + \pi/4$. We thus verify that the diagonal entries of σ_{x1} and σ_{x2} are all zero, which indicates that the linear longitudinal dephasing vanishes and the molecule is subject only to the second order, quadratic dephasing.

Our design can be regarded as an innovation of the N type system proposed in Ref. [41], where Rebić et. al have proposed to build an N level molecule by two capacitively coupled CPBs. In that situation, the N level structure is always symmetric on the optimal point. To get asymmetry, additionally DC charge bias was needed and only moderate $|E_{42} - E_{31}|$ can be obtained. Moreover, since the main decoherence source of the charge based superconducting circuits is the low-frequency charge noise, the DC bias in previous SPM scheme results longitudinal dephasing which severely damages the phase coherence of the molecule. Therefore, compared with previous design, our introduction of the coupling SQUID can offer more tunability and robustness to the artificial molecule.

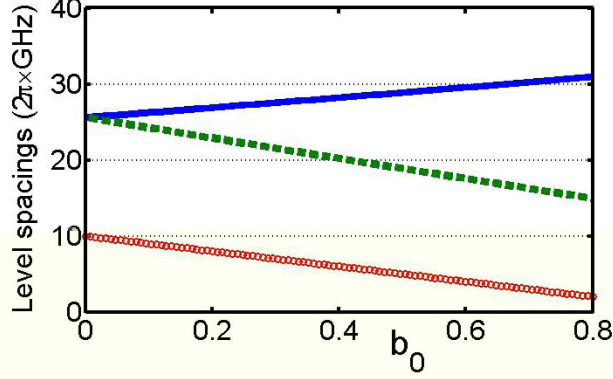


FIG. 4: (Color online). The level spacings versus b_0 . The solid, dashed, and round lines represent E_{31} , E_{42} , and E_{32} , respectively.

B. The classical pulse

We proceed to show how to implement the classical pumping connecting $|2\rangle$ and $|3\rangle$. Penetrating the external flux into the SQUID loops of the CPBs can couple microwave pulses with the molecule through the operators σ_{z1} and σ_{z2} , which have the matrix form

$$\sigma_{z1} = \begin{bmatrix} -\cos 2\theta & 0 & 0 & -\sin 2\theta \\ 0 & 0 & -1 & 0 \\ 0 & -1 & 0 & 0 \\ -\sin 2\theta & 0 & 0 & \cos 2\theta \end{bmatrix}, \quad (22)$$

$$\sigma_{z2} = \begin{bmatrix} -\cos 2\theta & 0 & 0 & -\sin 2\theta \\ 0 & 0 & 1 & 0 \\ 0 & 1 & 0 & 0 \\ -\sin 2\theta & 0 & 0 & \cos 2\theta \end{bmatrix}. \quad (23)$$

The matrix elements of σ_{z1} and σ_{z2} support the transitions inside the Hilbert subspaces $\text{span}\{|1\rangle, |4\rangle\}$ and $\text{span}\{|2\rangle, |3\rangle\}$. Therefore, we can apply an AC flux pulse to the SQUID loop of the first qubit to modulate E_{J1} with amplitude Ω_{Ex} and frequency ω_p . When ω_p is tuned close to E_{32} , the $|2\rangle \leftrightarrow |3\rangle$ transition is effectively induced while the $|1\rangle \leftrightarrow |4\rangle$ transition can be neglected due to frequency mismatch. To further suppress the unwanted $|1\rangle \leftrightarrow |4\rangle$ transition, we can synchronizely modulate E_{J2} with the same amplitude and

opposite phase as that of E_{J1} . In this way we get a pumping Hamiltonian

$$\begin{aligned} H_{pump} &= \Omega_{Ex} \cos \omega_P t (\sigma_{z1} - \sigma_{z2}) \\ &\cong -\Omega_{Ex} [\exp(i\omega_P t) |2\rangle \langle 3| + \exp(-i\omega_P t) |3\rangle \langle 2|] \end{aligned} \quad (24)$$

which establishes the pure $|2\rangle \leftrightarrow |3\rangle$ transition.

C. Coupling between the TLRs and the molecule

We consider the capacitive coupling between the TLRs and the molecule. As shown in Fig. 2, The TLR A (blue) has length L_A and fullwave frequency ω_A , while the TLR B (red) has length L_B and fullwave frequency ω_B . The Hamiltonian of the two individual TLRs are

$$H_{Cavity} = \omega_A a^\dagger a + \omega_B b^\dagger b, \quad (25)$$

where $\omega_{A,B} = 2\pi / (L_{A,B} \sqrt{Fc})$ are the eigenfrequencies, F and c being the inductance and capacitance per unit length, $L_{A,B}$ being the length of the two TLRs, and a, b are the annihilation operators of the fullwave modes, respectively. The quantized voltages of the TLRs are

$$\begin{aligned} V_A(x) &= \sqrt{\omega_A / L_A c} (a^\dagger + a) \cos(2\pi x / L_A), x \in [-L_A/2, L_A/2], \\ V_B(x) &= \sqrt{\omega_B / L_B c} (b^\dagger + b) \cos(2\pi x / L_B), x \in [-L_B/2, L_B/2]. \end{aligned} \quad (26)$$

When the two TLRs are capacitively connected with the molecule, the interaction Hamiltonian has the general form

$$H_{cc} = V_1 [C_{A1} V_A(x_{A1}) + C_{B1} V_B(x_{B1})] + V_2 [C_{A2} V_A(x_{A2}) + C_{B2} V_B(x_{B2})], \quad (27)$$

where the C_{Aj}, C_{Bj} for $j = 1, 2$ are the coupling capacitance between the j th qubit and the TLRs, the x_{Aj}, x_{Bj} for $j = 1, 2$ are the locations of the coupling capacitor, and $V_{1,2} = [C_\Sigma \sigma_{x1,2} + C_m \sigma_{x2,1}] / (C_\Sigma^2 - C_m^2)$ are the quantized voltages of the first and second CPB. We further expand H_{cc} as

$$\begin{aligned} H_{cc} &= h_{A1} (a^\dagger + a) \sigma_{x1} + h_{A2} (a^\dagger + a) \sigma_{x2} \\ &\quad + h_{B1} (b^\dagger + b) \sigma_{x1} + h_{B2} (b^\dagger + b) \sigma_{x2} \end{aligned} \quad (28)$$

where $h_{A,B;1,2}$ are the coupling factors which can be written as

$$h_{A,B;1,2} = \sqrt{\frac{\omega_{A,B}}{L_{A,B}C}} \frac{e}{(C_{\Sigma}^2 - C_m^2)} [C_{A,B;1,2} \cos\left(\frac{2\pi x_{A,B;1,2}}{L_{A,B}}\right) C_{\Sigma 2,1} + C_{A,B;2,1} \cos\left(\frac{2\pi x_{A,B;2,1}}{L_{A,B}}\right) C_m]. \quad (29)$$

The operators σ_{x1} and σ_{x2} have matrix elements which induce the transitions between subspace $\text{span}\{|1\rangle, |4\rangle\}$ and $\text{span}\{|2\rangle, |3\rangle\}$. We can thus tune the E_J and b_0 so that E_{42} and E_{31} are close to the cavity mode frequencies $\omega_{A,B}$. In this case the TLRs can effectively only induce the $|1\rangle \leftrightarrow |3\rangle$ and $|2\rangle \leftrightarrow |4\rangle$ transitions. The remaining $|1\rangle \leftrightarrow |2\rangle$ and $|3\rangle \leftrightarrow |4\rangle$ transitions are suppressed due to frequency selection. With the rotating wave approximation, H_{cc} finally reads

$$H_{cc} = g_{A1}(\sigma_{13}a^\dagger + \sigma_{31}a) + g_{B1}(\sigma_{13}b^\dagger + \sigma_{31}b) + g_{A2}(\sigma_{24}a^\dagger + \sigma_{42}a) + g_{B2}(\sigma_{24}b^\dagger + \sigma_{42}b), \quad (30)$$

where the coupling factors $g_{A,B;1,2}$ are

$$g_{A,B;1} = \cos \varphi (h_{A,B;1} + h_{A,B;2}), \quad (31)$$

$$g_{A,B;2} = \cos \varphi (h_{A,B;1} - h_{A,B;2}).$$

D. XPM in circuit QED

H_{cc} in Eq. (30) has a more general form than the atom-photon coupling terms in Eq. (3). The flexibility of superconducting devices allow us to choose suitable values and locations of the coupling capacitors in order to get desired coupling configurations. The setting of the locations of the capacitors does not require to put the CPBs in distant places, because the TLRs can be fabricated in a zig-zag form. A trivial case is that $C_{B1} = C_{B2} = 0$, i. e. the molecule is connected only to the TLR A, which results the SPM of circuit QED [41]. To establish the XPM described in Sec. II, we set the coupling capacitors to have capacitances $C_{B1} = C_{B2}$ and $C_{A1} = C_{A2}$. In addition, the location of the capacitors are selected as $x_{A1} = x_{A2} = 0$ and $x_{B1} = L_B/2 - x_{B2} = L_B/8$. In this way, $h_{A1} = h_{A2}$, $h_{B1} = -h_{B2}$ and the resulting H_{cc} is given by

$$H_{cc} = g_{A1}(\sigma_{13}a^\dagger + \sigma_{31}a) + g_{B2}(\sigma_{24}b^\dagger + \sigma_{42}b). \quad (32)$$

Up to a trivial i factor, H_{cc} in Eq. (32) has the same atom-photon coupling form as that of H_{int} in Eq. (3), i. e. the TLRs A and B replace the role of the cavities a_1 and a_2 , respectively.

Combining Eqs. (18), (24), and (32), We develop all the required elements of the N level XPM scheme in the circuit QED system. When we tune the classical pumping to be in dark resonance with the TLR A, an effective Kerr interaction hamiltonian

$$H_{eff} = -\frac{g_{B2}^2 g_{A1}^2}{\Delta \Omega_{Ex}^2} a^\dagger b^\dagger ab, \quad (33)$$

can be induced between the two TLRs.

The Kerr coefficient $\chi_3 = g_{A1}^2 g_{B2}^2 / (\Delta \Omega_{Ex}^2)$ can be estimated based on the reported experiments. Since the coupling strength between a TLR and a qubit as large as 300 MHz has been achieved, we set $g_1/2\pi = g_2/2\pi = 300$ GHz. In addition, the classical pumping strength Ω_{Ex} and the detuning $\Delta = E_{A2} - \omega_B$ can be chosen as $\Omega_{Ex}/2\pi = 1.5$ GHz and $\Delta/2\pi = 1.5$ GHz to fulfill the adiabatical condition in Eq. (4). We then get $\chi_3/2\pi \cong 2.5$ MHz, which has already exceeded the observed Kerr strength obtained by exploiting a large Josephson junction connected with the TLR in the recent papers [44–46].

IV. THE ROLE OF ATOMIC DECOHERENCE IN XPM,

We discuss the influence of molecule's decoherence on the XPM. As shown in Fig. 1, in the first step we consider only the decay processes $|3\rangle \rightarrow |1\rangle$, $|3\rangle \rightarrow |2\rangle$, and $|4\rangle \rightarrow |2\rangle$, with decay rates γ_1 , γ_2 , and γ_3 , respectively. In this case the polarizations $\langle \sigma_{13} \rangle_S$ and $\langle \sigma_{24} \rangle_S$ have the form

$$\begin{aligned} \langle \sigma_{13} \rangle_S &= -\frac{g_1 g_2^2}{(\gamma_3 + i\Delta) \Omega_c^2} a_2^\dagger a_1 a_2, \\ \langle \sigma_{24} \rangle_S &= -\frac{g_1^2 g_2}{(\gamma_3 + i\Delta) \Omega_c^2} a_1^\dagger a_1 a_2, \end{aligned} \quad (34)$$

which results a complex Kerr coefficient

$$\chi_3 = \frac{g_1^2 g_2^2}{(-i\gamma_3 + \Delta) \Omega_c^2}. \quad (35)$$

We notice that χ_3 does not depend on either γ_1 or γ_2 . In addition, the first order terms of $\langle \sigma_{13} \rangle_S$ and $\langle \sigma_{24} \rangle_S$ are still zero. These two effect can be explained by the EIT in the lowest levels of the molecule. The destructive interference between the $|3\rangle \leftrightarrow |1\rangle$ and $|3\rangle \leftrightarrow |2\rangle$

transition branches cancels the first order terms of $\langle\sigma_{13}\rangle_S$ and $\langle\sigma_{24}\rangle_S$ and thus the linear susceptibilities of the TLRs. Moreover, the coherent population trapping significantly suppress the population $\langle\sigma_{33}\rangle_S$. As a result, the decay channels $|3\rangle \leftrightarrow |1\rangle$ and $|3\rangle \leftrightarrow |2\rangle$ become irrelevant. Therefore, we use the relative decay rate R define by $R = |\Im(\chi_3)/\Re(\chi_3)|$ to characterize the molecule-induced cavity decay. Since $\gamma_3/2\pi$ has been pushed to the order of 0.5 MHz in recent experiments [8], while Δ can be usually set to be on the order of GHz, $R = \gamma_3/\Delta$ is estimated to be in the range $[10^{-3}, 10^{-4}]$.

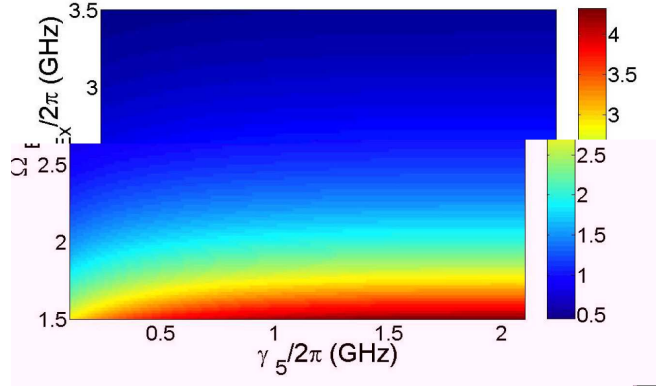


FIG. 5: (Color online). The Kerr nonlinearity $\chi'_3 = \Re(\chi_3)$ versus Ω_{Ex} and γ_5 .

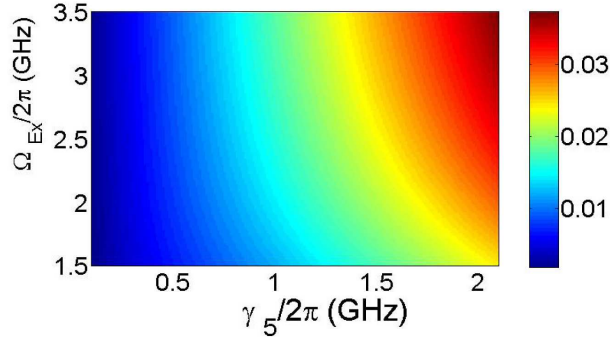


FIG. 6: (Color online). The linear dispersion factor χ'_1/χ'_3 versus Ω_{Ex} and γ_5 .

We further take the decay $|2\rangle \rightarrow |1\rangle$ and dephasing between $|2\rangle$ and $|1\rangle$ into account. The corresponding decoherence rates are γ_4 and γ_ϕ . These two processes can break the phase coherence between $|2\rangle$ and $|1\rangle$, which is essential in the previous suppression of linear dispersion and absorption. In this circumstance the first order of $\langle\sigma_{13}\rangle_S$ emerges. It takes the form

$$\sigma_{13}^1 = -\gamma_5 g_{A1} a / B, \quad (36)$$

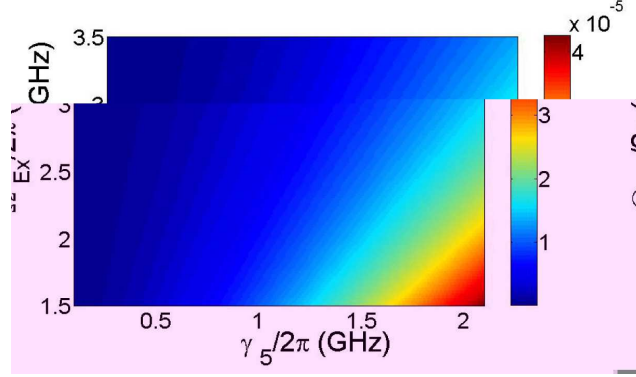


FIG. 7: (Color online). The linear absorption factor χ_1''/χ_3' versus Ω_{Ex} and γ_5 .

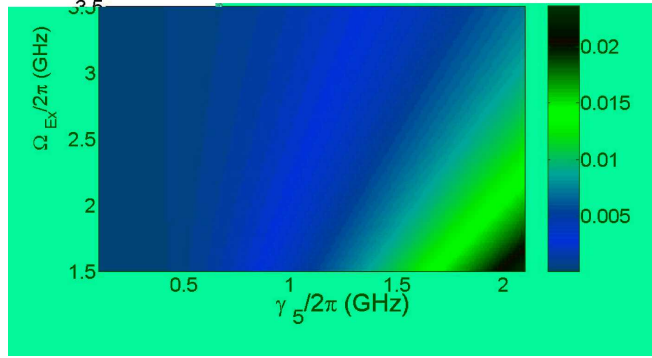


FIG. 8: (Color online). The nonlinear absorption factor $\Im(\chi_3)/\chi_3'$ versus Ω_{Ex} and γ_5 .

where $\gamma_5 = \gamma_4 + \gamma_\phi$ and $B = \Omega_{Ex}^2 + \gamma_1\gamma_5 + \gamma_2\gamma_5 + i\delta\gamma_5$. The resulting linear susceptibility is

$$\chi_1 = g_{A1}^2 \gamma_5 / B. \quad (37)$$

the real part χ_1' of χ_1 which describes the decoherence induced dispersion of the TLR A is approximately $g_{A1}^2 \gamma_5 / \Omega_{Ex}^2$. With $\gamma_5 / 2\pi \cong 0.5$ MHz, $\chi_1' / 2\pi$ is lower than 0.01 MHz. The imaginary part χ_1'' of χ_1 , which describes the decoherence induced dissipation of the TLR A, can be approximated as $\chi_1'' \cong g_{A1}^2 \gamma_5 \delta \gamma_5 / \Omega_{Ex}^4$. It is even smaller than χ_1' by several orders. The analytic form of χ_3 in the presence of the decoherence $|2\rangle \rightarrow |1\rangle$ and the dephasing becomes complicated. We thus numerically calculate the Kerr coefficient $\chi_3' = \Re(\chi_3)$ versus the pumping Ω_{Ex} and the decoherence rate γ_5 . The result is shown in Fig. 5. We find that χ_3' depends weakly on γ_5 . When γ_5 becomes non zero, $\chi_3' / 2\pi$ remains to be larger than 1 MHz. We further calculate the dispersion factor χ_1' / χ_3' , the linear absorption factor χ_1'' / χ_3' , and the nonlinear absorption factor $\Im(\chi_3) / \chi_3'$ and plot the results in Figs. 6, 7, and 8. We see that the unwanted effects increase rapidly with increasing γ_5 . Nevertheless, in the region

of current technology $\gamma_5/2\pi \cong 0.5$ MHz, these effects are still smaller than the XPM by at least two orders of magnitude. If the decoherence effects can be suppressed to the range $\gamma_5/2\pi \cong 0.1$ MHz in the future experiments, a more pure XPM with negligible dispersion and absorption can be achieved.

V. APPLICATIONS AND DISCUSSION

As mentioned in the previous section, the molecule induced fluctuation of the TLRs is approximately two to three orders lower than the cross Kerr nonlinearity which is on the level MHz. In addition, with current technology, the Q factor of a single TLR has already been pushed to the order of 10^6 [7], which yields the decay rate on the level 10 kHz. Since both the intrinsic decoherence of the TLRs and the molecule induced decoherence are all very small compared with the strength of Kerr nonlinearity, several important inter-TLR quantum operations in which only few photons are involved in each TLR could be realized with very high fidelities. Recently there are proposals of using the TLRs as qubits to realize scalable quantum computing [47, 48]. The TLR states with zero and one photon are used as the logical $|0\rangle$ and $|1\rangle$. Therefore, our proposed Kerr nonlinearity can obviously be exploited to establish the control phase gates in this system. Another application of the cross Kerr nonlinearity is the generation of the inter-TLR macroscopic maximal entangled cat state [49–51]. In the first step we tune the molecule decoupled with the TLRs. We then use classical pulses to pump the TLRs to the factorized coherent state $|\alpha\rangle_A |\beta\rangle_B$ and then adiabatically tune the molecule to establish XPM with strength χ_3 between the TLRs. After a time $t = \pi/\chi_3$, the initial $|\alpha\rangle_A |\beta\rangle_B$ evolves to a state

$$|\Psi\rangle = \frac{1}{2}(|\alpha\rangle_A |\beta\rangle_B + |-\alpha\rangle_A |\beta\rangle_B + |\alpha\rangle_A |-\beta\rangle_B - |-\alpha\rangle_A |-\beta\rangle_B) \quad (38)$$

Although the coherent states are not orthogonal, the overlap $|\langle\beta|\alpha\rangle|$ is only 10^{-7} for a moderate $|\beta - \alpha| = 4$. Superpositions of this kind have no classical counterpart and correspond to Schrödinger catlike states. Therefore, the state $|\Psi\rangle$ can be viewed as the macroscopic entangled cat state, which can be used as logical elements in quantum computation and can offer further insight into the boundary of classical-quantum worlds. We mention that since the coherent state spreads over the whole Fock space, such an entangled cat state can hardly be prepared by the generalized Eberly-Law algorithm, which has been used to generate the

NOON states in the circuit QED system [17, 18].

An alternative coupling configuration we can achieve is that the TLR A couples the $|1\rangle \leftrightarrow |3\rangle$ transition while the TLR B couples both the $|1\rangle \leftrightarrow |3\rangle$ and $|2\rangle \leftrightarrow |4\rangle$ transitions. The coupling between the TLR B and the $|1\rangle \leftrightarrow |3\rangle$ transition can result from either the intention of the experiment or the fabrication errors of the coupling capacitors. In this situation, the difference between the mode frequencies plays an important role. When $\omega_A = \omega_B$, an effective Hamiltonian

$$H_{eff} = -\frac{g_{B2}^2 g_{A1}^2}{\Delta \Omega_{Ex}^2} a^\dagger b^\dagger ab - \frac{g_{B2}^2 g_{B1}^2}{\Delta \Omega_{Ex}^2} b^\dagger b^\dagger bb, \quad (39)$$

in which the self Kerr effect and the cross Kerr effect co-exist is obtained. When $\omega_A \neq \omega_B$, since the TLR B is not resonant with the classical pumping field, it can hardly transfer population to the state $|2\rangle$, the effective TLR-TLR Hamiltonian thus remains the form $-g_{A1}^2 g_{B2}^2 a^\dagger b^\dagger ab / (\Delta \Omega_{Ex}^2)$. From this point of view, it is favorable to use TLRs with different eigenfrequencies to realize the XPM, since the difference of their frequencies makes the scheme more robust against the fabrication errors.

Recently theoretical and experimental works have suggested that the large Josephson junction can be used to produce SPM and XPM for the TLRs [44–46, 48]. By connecting a large Josephson junction with the TLRs, one can obtain the Kerr nonlinearity from the Taylor expansion of the Josephson energy up to the fourth order. The Kerr nonlinearity obtained in this way is smaller than what we have proposed, often on the order of hundreds of kHz. Moreover, the critical current noise and the flux noise in the large Josephson junction results large fluctuations of the Josephson energy and consequently the severe linear dispersion of the TLRs. To eliminate the effect of the fluctuation, one have to use additional spin-echo like technique [48] which complicate the quantum gate sequence. Compared with these schemes, our alternative XPM scheme may be more robust against the noises and may offer more pure Kerr nonlinearity with suppressed frequency drifts.

VI. CONCLUSION

In conclusion, in this paper we have shown that an “artificial” multilevel system in circuit QED produces the effective XPM between two TLRs with strength much larger than previously known. The obtained XPM is very robust against the noises in solid state sys-

tem. Compared with the XPM strength, the accompanying dispersion and absorption is negligible. Various QIPs can be implemented in this architecture. This work may offer improvement to the future scalable quantum computation in superconducting devices.

Acknowledgments

We thank Prof. Y. F. Zhu, S. Rebić, Z. W. Zhou, and Y. F. Xiao for fruitful discussions. This work is funded by the start funding of HUST, No. 01-24-012018 and No. 01-24-012030, the Natural Science Foundation of Hubei province, and the National Natural Science Foundation of China, Grant No. 60871018.

Appendix A: The effective XPM Hamiltonian

The derivation of Eqs. (10) and (11) is provided in this Appendix. As shown in Fig. 1, taking the decoherence processes $|3\rangle \rightarrow |1\rangle$, $|3\rangle \rightarrow |2\rangle$, and $|4\rangle \rightarrow |2\rangle$ of the atom and the decay of the two cavities into account, we write the system-bath Hamiltonian as

$$H_{whole} = H_{sys} + H_{bath}, \quad (\text{A1})$$

where H_{damp} represents the coupling of the system to reservoir mediating cavity decay and spontaneous emission; it takes the form [33]

$$\begin{aligned} H_{damp} = & \sum_{j=1,2,-\infty}^{+\infty} \int \omega b_j^\dagger(\omega) b_j(\omega) d\omega + \sum_{j=1,2,3,-\infty}^{+\infty} \int \omega \beta_j^\dagger(\omega) \beta_j(\omega) d\omega \\ & + \sum_{j=1,2,-\infty}^{+\infty} \int i \sqrt{\frac{\kappa_j}{\pi}} [b_j^\dagger(\omega) a_j - a_j^\dagger b_j(\omega)] d\omega \\ & + \int_{-\infty}^{+\infty} i \sqrt{\frac{\gamma_1}{\pi}} [\beta_1^\dagger(\omega) \sigma_{13} - \sigma_{31} \beta_1(\omega)] d\omega \\ & + \int_{-\infty}^{+\infty} i \sqrt{\frac{\gamma_2}{\pi}} [\beta_2^\dagger(\omega) \sigma_{23} - \sigma_{32} \beta_2(\omega)] d\omega \\ & + \int_{-\infty}^{+\infty} i \sqrt{\frac{\gamma_3}{\pi}} [\beta_3^\dagger(\omega) \sigma_{24} - \sigma_{42} \beta_3(\omega)] d\omega, \end{aligned} \quad (\text{A2})$$

with $\{b_j(\omega), \beta_j(\omega)\}$ the reservoir's annihilation operators at frequency ω and $\{\kappa_j, \gamma_j\}$ the corresponding decoherence rates. Here we have made the Markovian approximation that the system-bath coupling coefficients are constant around the frequencies of interest.

The master equation of the density matrix ρ of the system is

$$\begin{aligned} \frac{d\rho}{dt} = & i[\rho, H_{sys}] + \kappa_1 L[a_1]\rho + \kappa_2 L[a_2]\rho \\ & + \gamma_1 L[\sigma_{13}]\rho + \gamma_2 L[\sigma_{23}]\rho + \gamma_3 L[\sigma_{24}]\rho, \end{aligned} \quad (\text{A3})$$

where $L[c]\rho = 2c\rho c^\dagger - c^\dagger c\rho - \rho c^\dagger c$ is the Lindbladian form. The expectation value $\langle O \rangle$ of a particular system operator O thus evolves as

$$\frac{d\langle O \rangle}{dt} = \text{Tr}(O \frac{d\rho}{dt}) = \langle K \rangle, \quad (\text{A4})$$

where

$$\begin{aligned} K = & i[H_{sys}, O] + \kappa_1 M[a_1]O + \kappa_2 M[a_2]O \\ & + \gamma_1 M[\sigma_{13}]O + \gamma_2 M[\sigma_{23}]O + \gamma_3 M[\sigma_{24}]O, \end{aligned} \quad (\text{A5})$$

with the M form $M[c]O = 2c^\dagger O c - c^\dagger c O - O c^\dagger c$. With the help of Eq. (A4), we calculate the time evolution of all the expectation values of the atomic operators. The evolution equations of the population operators are

$$\frac{d\langle \sigma_{11} \rangle}{dt} = \left\langle g_1 \left(a_1^\dagger \sigma_{13} + \sigma_{31} a_1 \right) + 2\gamma_1 \sigma_{33} \right\rangle, \quad (\text{A6})$$

$$\begin{aligned} \frac{d\langle \sigma_{22} \rangle}{dt} = & \left\langle g_2 \left(a_2^\dagger \sigma_{24} + \sigma_{42} a_2 \right) + 2\gamma_3 \sigma_{44} \right\rangle \\ & + \langle \Omega_c (\sigma_{23} + \sigma_{32}) + 2\gamma_2 \sigma_{33} \rangle, \end{aligned} \quad (\text{A7})$$

$$\begin{aligned} \frac{d\langle \sigma_{33} \rangle}{dt} = & - \left\langle \left\{ g_1 \left(a_1^\dagger \sigma_{13} + \sigma_{31} a_1 \right) + 2\gamma_1 \sigma_{33} \right\} \right\rangle \\ & - \langle \Omega_c (\sigma_{23} + \sigma_{32}) + 2\gamma_2 \sigma_{33} \rangle, \end{aligned} \quad (\text{A8})$$

$$\frac{d\langle \sigma_{44} \rangle}{dt} = - \left\langle \left\{ g_2 \left(a_2^\dagger \sigma_{24} + \sigma_{42} a_2 \right) + 2\gamma_3 \sigma_{44} \right\} \right\rangle, \quad (\text{A9})$$

while the evolution equations of the coherence operators are

$$\frac{d\langle \sigma_{12} \rangle}{dt} = \langle \Omega_c \sigma_{13} \rangle + \left\langle g_1 \sigma_{32} a_1 + g_2 a_2^\dagger \sigma_{14} \right\rangle, \quad (\text{A10})$$

$$\begin{aligned} \frac{d\langle\sigma_{13}\rangle}{dt} &= \langle -(\gamma_1 + \gamma_2 + i\delta)\sigma_{13} - \Omega_c\sigma_{12} \rangle \\ &\quad + \langle g_1(\sigma_{33} - \sigma_{11})a_1 \rangle, \end{aligned} \quad (\text{A11})$$

$$\frac{d\langle\sigma_{14}\rangle}{dt} = \langle -(\gamma_3 + i\Delta)\sigma_{14} \rangle + \langle g_1\sigma_{34}a_1 - g_2\sigma_{12}a_2 \rangle, \quad (\text{A12})$$

$$\begin{aligned} \frac{d\langle\sigma_{32}\rangle}{dt} &= \langle (-\gamma_1 - \gamma_2 + i\delta)\sigma_{32} + \Omega_c(\sigma_{33} - \sigma_{22}) \rangle \\ &\quad + \langle g_2a_2^\dagger\sigma_{34} - g_1a_1^\dagger\sigma_{12} \rangle, \end{aligned} \quad (\text{A13})$$

$$\frac{d\langle\sigma_{24}\rangle}{dt} = \langle -(\gamma_3 + i\Delta)\sigma_{24} + \Omega_c\sigma_{34} \rangle + \langle g_2(\sigma_{44} - \sigma_{22})a_2 \rangle, \quad (\text{A14})$$

$$\begin{aligned} \frac{d\langle\sigma_{34}\rangle}{dt} &= \langle -(\gamma_1 + \gamma_2 + \gamma_3 - i\delta + i\Delta)\sigma_{34} - \Omega_c\sigma_{24} \rangle \\ &\quad - \langle (g_1a_1^\dagger\sigma_{14} + g_2\sigma_{32}a_2) \rangle. \end{aligned} \quad (\text{A15})$$

When the adiabatic conditions in Eq. (4) are fulfilled, the degrees of freedom of the atom follow those of the cavities. Therefore, we set the right side of Eqs. (A6)-(A15) to be zero and represent the atomic operators by the annihilation and creation operators of the cavities. Suppose initially the atom is prepared in its ground state $|1\rangle$, we can choose $\langle\sigma_{11}\rangle = 1$ as a meaningful start and solve the Eqs. (A6)-(A15) iteratively. The stationary values up to the third order of the iteration are

$$\begin{aligned} \langle\sigma_{11}\rangle_S &= 1 - \frac{g_1^2}{\Omega_c^2}a_1^\dagger a_1, \quad \langle\sigma_{22}\rangle_S = \frac{g_1^2}{\Omega_c^2}a_1^\dagger a_1, \\ \langle\sigma_{33}\rangle_S &= \langle\sigma_{44}\rangle_S = 0, \end{aligned} \quad (\text{A16})$$

$$\begin{aligned} \langle\sigma_{12}\rangle_S &= -\frac{g_1}{\Omega_c}a_1 + \frac{g_1^3}{\Omega_c^3}a_1^\dagger a_1 a_1 + \frac{(\gamma_1 + \gamma_2 + i\delta)g_1g_2^2}{(\gamma_3 + i\Delta)\Omega_c^3}a_2^\dagger a_1 a_2, \\ \langle\sigma_{13}\rangle_S &= -\frac{g_1g_2^2}{(\gamma_3 + i\Delta)\Omega_c^2}a_2^\dagger a_1 a_2, \quad \langle\sigma_{14}\rangle_S = \frac{g_1g_2}{(\gamma_3 + i\Delta)\Omega_c}a_1 a_2, \\ \langle\sigma_{32}\rangle_S &= \langle\sigma_{34}\rangle_S = 0, \quad \langle\sigma_{24}\rangle_S = -\frac{g_1^2g_2}{(\gamma_3 + i\Delta)\Omega_c^2}a_1^\dagger a_1 a_2. \end{aligned} \quad (\text{A17})$$

Setting $\gamma_3 = 0$ we get Eqs. 10 and 11 from Eq. A17.

In this Appendix, we have treated a relative simple case. Only few decoherence channels are involved, while the atom-photon coupling configuration is also very "clean". For the more complicated situations discussed in the manuscript, this systematic method is still valid: We first modify H_{whole} according to the problems we consider and then re-derive the

evolution equations for the atomic operators; After performing the adiabatical elimination and iteration, we can get the stationary values of the atomic operators which contain the information of the effective evolution of the two cavity modes.

-
- [1] A. Blais, R. S. Huang, A. Wallraff, S. M. Girvin, and R. J. Schoelkopf, *Phys. Rev. A* **69**, 062320 (2004).
 - [2] A. Wallraff, D. I. Schuster, A. Blais, L. Frunzio, R. S. Huang, J. Majer, S. Kumar, S. M. Girvin, and R. J. Schoelkopf, *Nature (London)* **431**, 162 (2004).
 - [3] Y. Makhlin, G. Schon, and A. Shnirman, *Rev. Mod. Phys.* **73**, 357 (2001).
 - [4] M. H. Devoret, A. Wallraff, and J. M. Martinis, e-print arXiv:cond-mat/0411174.
 - [5] J. Clarke and F. K. Wilhelm, *Nature (London)* **453**, 1031 (2008).
 - [6] J. M. Raimond, M. Brune, and S. Haroche, *Rev. Mod. Phys.* **73**, 565 (2001).
 - [7] L. Frunzio, A. Wallraff, D. I. Schuster, J. Majer, and R. J. Schoelkopf, *IEEE Trans. Appl. Supercond.* **15**, 860 (2005).
 - [8] J. A. Schreier, A. A. Houck, Jens Koch, D. I. Schuster, B. R. Johnson, J. M. Chow, J. M. Gambetta, J. Majer, L. Frunzio, M. H. Devoret, S. M. Girvin, and R. J. Schoelkopf, *Phys. Rev. B* **77**, 180502 (2008).
 - [9] A. A. Houck, D. I. Schuster, J. M. Gambetta, J. A. Schreier, B. R. Johnson, J. M. Chow, L. Frunzio, J. Majer, M. H. Devoret, S. M. Girvin, and R. J. Schoelkopf, *Nature (London)* **449**, 328 (2007).
 - [10] Mika A. Sillanpää, J. I. Park, and R. W. Simmonds, *Nature (London)* **449**, 438 (2007).
 - [11] J. Majer, J. M. Chow, J. M. Gambetta, J. Koch, B. R. Johnson, J. A. Schreier, L. Frunzio, D. I. Schuster, A. A. Houck, A. Wallraff, A. Blais, M. H. Devoret, S. M. Girvin, and R. J. Schoelkopf, *Nature (London)* **449**, 443 (2007).
 - [12] M. Hofheinz, H. Wang, M. Ansmann, R. C. Bialczak, E. Lucero, M. Neeley, A. D. O'Connell, D. Sank, J. Wenner, J. M. Martinis, and A. N. Cleland, *Nature (London)* **459**, 549 (2009).
 - [13] H. Wang, M. Hofheinz, M. Ansmann, R. C. Bialczak, Erik Lucero, M. Neeley, A. D. O'Connell, D. Sank, M. Weides, J. Wenner, A. N. Cleland, and J. M. Martinis, *Phys. Rev. Lett.* **103**, 200404 (2009).
 - [14] R. S. Huang, Ph.D. thesis, Indiana University, 2004 (unpublished).

- [15] Y. Hu, Y. F. Xiao, Z. W. Zhou, and G. C. Guo, *Phys. Rev. A* **75**, 012314 (2007).
- [16] M. Mariani, F. Deppe, A. Marx, R. Gross, F. K. Wilhelm, and E. Solano, *Phys. Rev. B* **78**, 104508 (2008).
- [17] F. W. Strauch, K. Jacobs, and R. W. Simmonds, *Phys. Rev. Lett.* **105**, 050501 (2010).
- [18] H. Wang, Matteo Mariani, R. C. Bialczak, M. Lenander, E. Lucero, M. Neeley, A. O'Connell, D. Sank, M. Weides, J. Wenner, T. Yamamoto, Y. Yin, J. Zhao, J. M. Martinis, and A. N. Cleland, arXiv:1011.2862 (2010).
- [19] S. Rebić, Ph.D. thesis, University of Auckland, 2001 (unpublished).
- [20] D. F. Walls and G. J. Milburn, *Quantum Optics*, 2nd ed (Springer, Berlin 2008).
- [21] Q. A. Turchette, C. J. Hood, W. Lange, H. Mabuchi, and H. J. Kimble, *Phys. Rev. Lett.* **75**, 4710 (1995).
- [22] S. Rebić, A. S. Parkins, and S. M. Tan, *Phys. Rev. A* **65**, 063804 (2002).
- [23] A. Joshi and M. Xiao, *Phys. Rev. A* **72**, 062319 (2005).
- [24] M. D. Lukin and A. Imamoglu, *Phys. Rev. Lett.* **84**, 1419 (2000).
- [25] S. D. Barrett, Pieter Kok, Kae Nemoto, R. G. Beausoleil, W. J. Munro, and T. P. Spiller, *Phys. Rev. A* **71**, 060302(R) (2005).
- [26] H. Schmidt and A. Imamoglu, *Opt. Lett.* **21**, 1936 (1996).
- [27] H. Kang and Y. Zhu, *Phys. Rev. Lett.* **91**, 093601 (2003).
- [28] Y. F. Chen, C. Y. Wang, S. H. Wang, and I. A. Yu, *Phys. Rev. Lett.* **96**, 043603 (2006)
- [29] S. J. Li, X. D. Yang, X. M. Cao, C. H. Zhang, C. D. Xie, and H. Wang, *Phys. Rev. Lett.* **101**, 073602 (2008).
- [30] A. Imamoglu, H. Schmidt, G. Woods, and M. Deutsch, *Phys. Rev. Lett.* **79**, 1467 (1997).
- [31] P. Grangier, D. F. Walls, and K. M. Gheri, *Phys. Rev. Lett.* **81**, 2833 (1998).
- [32] A. Imamoglu, H. Schmidt, G. Woods, and M. Deutsch, *Phys. Rev. Lett.* **81**, 2836 (1998).
- [33] C. W. Gardiner and P. Zoller, *Quantum Noise*, (Springer, Berlin 2004), 2nd ed.
- [34] Y. F. Xiao, X. B. Zou, Z. F. Han, and G. C. Guo, *Phys. Rev. A* **74**, 044303 (2006).
- [35] M. O. Scully and M. S. Zubairy, *Quantum Optics*, 1st ed (Cambridge University Press 1997).
- [36] Y. Nakamura, Yu. A. Pashkin, and J. S. Tsai, *Nature (London)* **398**, 786 (1999).
- [37] M. Tinkham, *Introduction to Superconductivity*, 2nd ed. (McGraw-Hill, New York, 1996).
- [38] Y. Makhlin, G. Schön, and A. Shnirman, *Nature (London)* **398**, 305 (1999).
- [39] Y. A. Pashkin, T. Yamamoto, O. Astafiev, Y. Nakamura, D. V. Averin, and J. S. Tsai, *Nature*

- (London) **421**, 823 (2003)
- [40] T. Yamamoto, Y. A. Pashkin, O. Astafiev, Y. Nakamura, and J. S. Tsai, *Nature (London)* **425**, 941 (2003).
- [41] S. Rebić, J. Twamley, and G. J. Milburn, *Phys. Rev. Lett.* **103**, 150503 (2009).
- [42] D. Vion, A. Aassime, A. Cottet, P. Joyez, H. Pothier, C. Urbina, D. Esteve, and M. H. Devoret, *Science* **296**, 866 (2002).
- [43] G. Ithier, E. Collin, P. Joyez, P. J. Meeson, D. Vion, D. Esteve, F. Chiarello, A. Shnirman, Y. Makhlin, J. Schrieffer, and G. Schön, *Phys. Rev. B* **72**, 134519 (2005).
- [44] O. Suchoi, B. Abdo, E. Segev, O. Shtempluck, M. P. Blencowe, and E. Buks, *Phys. Rev. B* **81**, 174525 (2010).
- [45] S. Kumar and D. P. DiVincenzo, *Phys. Rev. B* **82**, 014512 (2010).
- [46] F. R. Ong, M. Boissonneault, F. Mallet, A. Palacios-Laloy, A. Dewes, A. C. Doherty, A. Blais, P. Bertet, D. Vion, and D. Esteve, e-print arXiv:1010. 6248 (2010).
- [47] M. Mariani, F. Deppe, A. Marx, R. Gross, F. K. Wilhelm, and E. Solano, *Phys. Rev. B* **78**, 104508 (2008);
- [48] L. H. Du, Y. Hu, Z. W. Zhou, G. C. Guo, and X. X. Zhou, *New J. Phys.* **12**, 063015 (2010).
- [49] B. C. Sanders, *Phys. Rev. A* **45**, 6811 (1992).
- [50] M. D. Lukin and A. Imamoglu, *Phys. Rev. Lett.* **84**, 1419 (2000).
- [51] S. Glancy and H. M. de Vasconcelos, *J. Opt. Soc. Am. B* **25**, 712 (2008).
- [52] J. Schrieffer, Ph.D. thesis, Universitat Karlsruhe (TH), 2005 (unpublished).